APPLIED SCIENCES AND ENGINEERING

Unique ion rectification in hypersaline environment: A high-performance and sustainable power generator system

Xuanbo Zhu[1], Junran Hao[2], Bin Bao[2], Yahong Zhou[3]*, Haibo Zhang[1], Jinhui Pang[1], Zhenhua Jiang[1]*, Lei Jiang[2,3]

The development of membrane science plays a fundamental role in harvesting osmotic power, which is considered a future clean and renewable energy source. However, the existing designs of the membrane cannot handle the low conversion efficiency and power density. Theory has predicted that the Janus membrane with ionic diode–type current would be the most efficient material. Therefore, rectified ionic transportation in a hypersaline environment (the salt concentration is at least 0.5 M in sea) is highly desired, but it still remains a challenge. Here, we demonstrate a versatile strategy for creating a scale-up Janus three-dimensional (3D) porous membrane–based osmotic power generator system. Janus membranes with tunable surface charge density and porosity were obtained by compounding two kinds of ionomers. Under electric fields or chemical gradients, the Janus membrane has ionic current rectification properties and anion selectivities in a hypersaline environment. Experiments and theoretical calculation demonstrate that abundant surface charge and narrow pore size distribution benefit this unique ionic transport behavior in high salt solution. Thus, the output power density of this membrane-based generator reaches 2.66 W/m^2 (mixing seawater and river water) and up to 5.10 W/m^2 at a 500-fold salinity gradient (i.e., flowing salt lake into river water). Furthermore, a generator, built by connecting a series of membranes, could power a calculator for 120 hours without obvious current decline, proving the excellent physical and chemical stabilities. Therefore, we believe that this work advances the fundamental understanding of fluid transport and materials design as a paradigm for a high-performance energy conversion generator.

INTRODUCTION

"Blue energy" collected from the osmotic difference between seawater and fresh water has been extensively studied as a clean, renewable, and sustainable power generation source (*1*–*5*). In 1954, Pattle (*6*) pointed out that Gibbs' free energy was lost when the sea meets the river. This kind of energy was not used until 1975 by Loeb and Norman (*7*) through selectively permeable membranes. Over the past decades, scientists have explored a wide range of membrane-based energy-harvesting technologies (*2*, *8*). Two main approaches, pressure-retarded osmosis (PRO) and reverse electrodialysis (RED), have been considered as sustainable methodologies (*9*–*12*). As for the RED method, osmotic energy could directly be converted into electric current. In traditional RED, ions are driven across a stack of alternating cation- and anion-selective membranes under a salt concentration gradient. Inspired by the electric eel that can generate 600 V, the conventional design principle for the membrane is the selectivity of single-layer membranes. Thus, nanofluidic-type membranes have been developed, covering inorganic membrane (e.g., boron nitride), organic membrane (e.g., graphene oxides and polymer) (*13*, *14*), and soft matter (e.g., hydrogel) (*15*). However, these generators are restrictive due to their inadequate mass ion streams (extremely small pore size that is generally sub–1 nm) or the large resistance within the membrane itself (*16*, *17*). So far, the maximum power density could reach up to 2.2 W/m^2 by large-scale tandem stacks (*2*, *8*), which is far from marginal for the industrial development requirement (the critical power density is 5.0 W/m^2 for the seawater/fresh water systems). This is due to (i) poor energy conversion efficiency, (ii) low output power density, and (iii) difficulty in scaling up membrane nanomanufacturing.

First, the polarization phenomenon during the conversion process causes energy loss and is the major hindrance of energy conversion efficiency. When the generator is applied to an external load resistance and the internal resistance of the membrane is equal to the load resistance, the maximum extractable power is reached. This predicts that most of the energy is lost within the membrane itself and dissipated as Joule heating between the pores (*18*). Nonlinear (ionic diode–type) current allows one-way ion transport, while the back current is blocked under a reverse bias. Therefore, the energy conversion efficiency can be boosted by an ionic diode–type membrane with asymmetric structure (*18*–*20*). However, to maintain high efficiency in the long run, the current in high salt concentration should be kept in the blocking regime because the salt concentration at sea is at least 0.5 M. However, the rectification phenomena are highly dependent on the ionic concentration, and the highest rectification ratio (defined as the ratio of currents measured at opposite voltages of the same magnitude) generally appeared at low concentration (less than 0.1 M) (*21*–*23*). At extremely high ionic concentration, rectified currents do not exist, and those with low rectification ratio of the surface charges are screened. During the energy conversion process, to avoid the current from switching back to the linear behavior, it is highly desirable to render the membrane-rectifying current in a hypersaline environment.

Second, the poor output power density is restricted by the ionic conductance that is dominated by the surface charge density and the internal resistance of the membrane (extremely small pore size

[1]National and Local Joint Engineering Laboratory for Synthetic Technology of High Performance Polymer, College of Chemistry, Jilin University, Changchun 130012, P. R. China. [2]Beijing Advanced Innovation Center for Biomedical Engineering, Beihang University, Beijing 100191, P. R. China. [3]CAS Key Laboratory of Bio-inspired Materials and Interfacial Science, Technical Institute of Physics and Chemistry, Chinese Academy of Sciences, Beijing 100190, P. R. China.
*Corresponding author. Email: zhouyh@mail.ipc.ac.cn (Y.Z.); jiangzhenhua@jlu.edu.cn (Z.J.)

and long pathway along the channels). Another crucial factor for the large-scale viability is the scale-up membrane with mechanical properties. For example, the boron nitride nanotube membrane reported by Siria *et al.* (*24*) showed excellent results in osmotic energy harvesting due to the high surface charge. However, large-scale viability still remains a great challenge, limiting its practical application.

To overcome these bottlenecks of the conventional membrane-based osmotic power generator, we designed a Janus three-dimensional (3D) porous membrane with tunable surface charge and porosity. On the basis of structure-property relationship, exquisite membranes with 3D uniform pore structure are prepared through the self-assembly route, which could be readily scaled up in a facile approach (Fig. 1A). We design and synthesize two ionomers, negatively charged hexasulfonated poly(aryl ether ketone)s (PAEK-HS) and positively charged poly(ether sulfone)s with pyridine pendants (PES-Py), as shown in Fig. 1, B and D, respectively. By tuning the pendants of the ionomers and using the phase-separation approach, we obtained a positively charged membrane with a pore size of 8.50 ± 2.37 nm and a porosity of 13.82 ± 1.37% and a negatively charged membrane with a pore size of 17.05 ± 6.06 nm and a porosity of 22.4 ± 1.9%. Thus, the large-scale Janus membrane with a thickness of 11 μm (1 μm of PES-Py and 10 μm of PAEK-HS) was prepared by spin-coating the PES-Py membrane to the PAEK-HS membrane, which was prepared by the solution-casting method (Fig. 1A and fig. S1). The as-prepared Janus membrane is fixed between two asymmetric salt solution reservoirs as a separator (Fig. 1E). Driven by the transmembrane chemical gradient, charged ions with one polarity are carried through the membrane, as other types of ions with opposite charge polarity are screened by the ion-selective Janus membrane with abundant surface charge. A net current is then generated. Meanwhile, this diode-type membrane blocks any current that flows back into the membrane. The efficiency is thus further improved. Output power densities of 2.66 W/m^2 (by mixing seawater and river water with 35.7% conversion efficiency) and 5.10 W/m^2 (at a 500-fold salinity gradient) are achieved. The designed Janus membrane holds unique features: (i) tunable surface charge density and porosity benefiting the ionic transmembrane conductivity (*25*, *26*); (ii) rectified current and ion selectivity maintained in extremely high salt solution, improving the conversion efficiency; and (iii) excellent robustness and facile to be scaled up. The numerical simulation predicts that abundant surface charge and small pore size with narrow distribution benefit the ionic current rectification (ICR) and excellent selectivity in a hypersaline

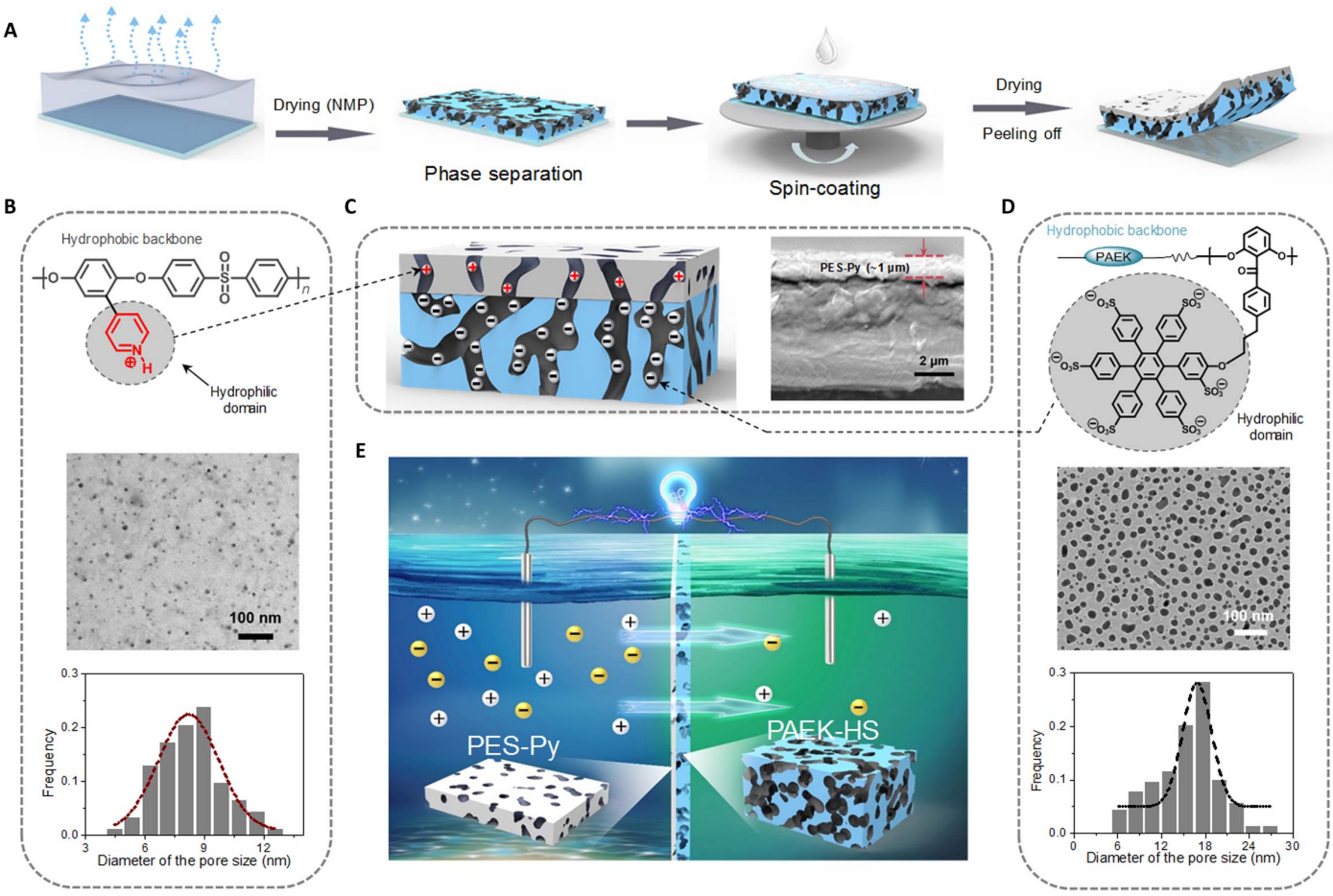

Fig. 1. Schematic depiction of the Janus 3D porous membrane–based osmotic power generator. (**A**) Preparation process of the Janus nanoporous membrane. (**B** and **D**) Chemical structure (top), microstructure of ionomers (middle), and statistics of pore size and Gauss fitting profile (bottom). The ionomers are PES-Py and PAEK-HS. (**C**) Schematic (left) and scanning electron microscopy observation (right) of the cross section of the asymmetric structure with 3D pores. The thickness of the PES-Py layer is about 1 μm. (**E**) Schematic depiction of the harvesting osmotic energy process under a concentration gradient based on the Janus 3D porous membrane.

environment. This Janus membrane design would boost power generator material development and provide a practical guide for porous membrane construction.

RESULTS

Porous membrane preparations

The energy conversion involves the fundamental ionic transport through the nanoscale-confined pores. To investigate the effect of surface charge on conductance and ICR, we designed a series of copolymer PAEK-HS bearing tuned pendant proportion (scheme S1). The monomer was synthesized via Williamson reaction. By regulating the ratio of monomers, we obtained a series of copolymers through nucleophilic substitution polycondensation reaction. Subsequently, target copolymers were prepared by a post-sulfonation reaction using chlorosulfonic acid. Here, the target copolymers were named as HS10, HS15, and HS20, where 10, 15, and 20, respectively, refer to the molar percentage of the hexaphenylbenzene monomer in the total difluoride monomer.

The successful syntheses were confirmed by ^{1}H NMR (nuclear magnetic resonance) and Fourier transform infrared (FT-IR) characterization (figs. S2 to S6). With the phase-separation approach (*23*, *27*, *28*), the well-defined ~17-nm 3D pores are self-assembled, which are directly read through the transmission electron microscopy (TEM) images (Fig. 2D and fig. S7). The surface charge density increases notably by increasing the pendant proportion, which was proved by zeta potential characterization and ion exchange capacity values (figs. S8 and S9). We also noted that the porosity of HS20 increased by 94% compared to that of HS10, while the pore size stays almost the same due to the intramolecular interactions inside the amphiphilic copolymer. With an exquisite chemical design, a well-defined 3D porous membrane with modulated surface charge density and porosity can be obtained. This approach may be proven useful for future porous material designs.

Subsequently, PES-Py with ca. 8-nm pores was synthesized by introducing a relative smaller pyridine pendant into PES. In addition, the as-obtained two ionomers could self-assemble into a porous membrane with well-defined 3D pores through phase separation. A large-scale Janus membrane composed of opposite charges and different pore sizes was prepared by spin-coating the PES-Py onto the PAEK-HS membrane, which was obtained by the solution-casting method.

Charge density affects the ionic transmembrane properties

During the conversion process in traditional RED, the energy is lost because of polarization phenomenon in the single-layer membrane system. By connecting electrodes in the reservoir to an external load resistance, the generated electric power can be collected. The maximum extractable power P_{max} is found when using the equivalent electric circuit: $P_{max} = R_M I^2_{osmosis}/4$, where R_M is the ionic internal resistance of the membrane and $I_{osmosis}$ is the generated current density. When the membrane is in contact with a load resistance (R_L) associated with the device used to extract the generated power, the maximum extractable power appears when $R_L = R_M$. This predicts that most of the osmotic power is dissipated within the membrane itself as the Joule heating between the pores. Diode-type current as nonlinear current could avoid this energy loss, as the back current is blocked under reverse bias (*18*). The diode current–type membrane that works in high salt concentration is desired to improve the efficiency of the generators, as the ionic concentration of the salt is at least 0.5 M.

ICR properties highly affect the ionic transport direction and are dependent on surface charge density (*29*–*36*). The surface charge density benefits the conductance because it affects the Dukhin length (the contribution of the surface conductivity to bulk conductivity)

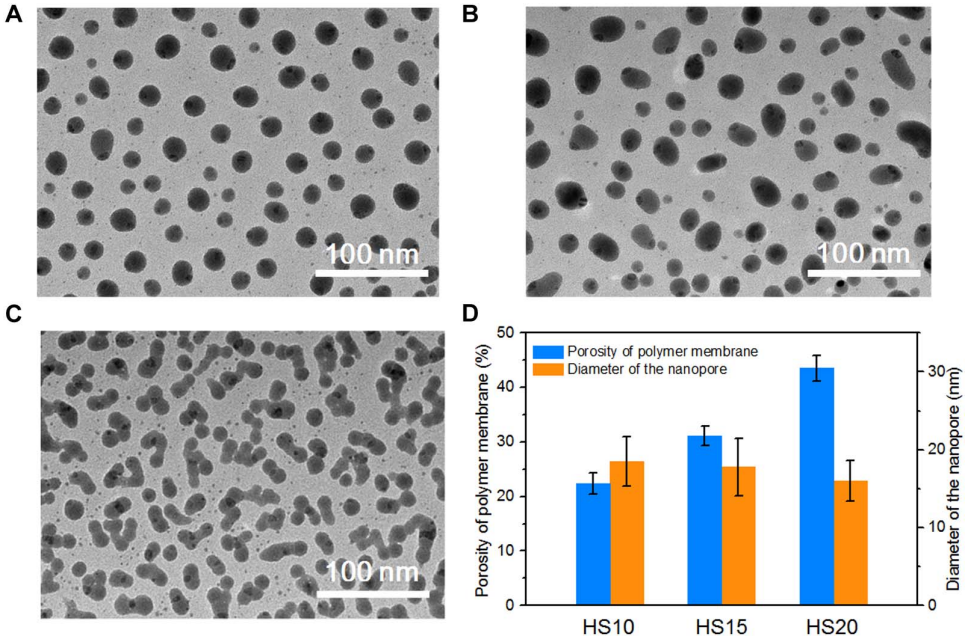

Fig. 2. Microscopic appearance characterization of PAEK-HS with tuned pendant proportion. (**A** to **C**) TEM images of HS10, HS15, and HS20. The copolymers were marked with $AgNO_3$, which reacted with the sulfonic acid moiety. Dark areas refer to pores formed by the hydrophilic pendants, and light areas represent the hydrophobic backbone. (**D**) Porosity and diameters of the copolymer membranes. While the pore size is well-defined uniform, the porosity of the polymer membrane is enlarged with the increasing pendant proportion. The statistics were obtained from the TEM images.

(*25*). By modulating the pendant proportion, the conductivity of membranes improves and shows the salt concentration dependence (Fig. 3A). Then, we explore the ICR property through the as-prepared Janus membrane in salt solution. The rectification ratio varies at different concentrations. Unexpectedly, the Janus membrane showed the highest rectification ratio (ca. 57.2) in 1 M KCl solution, and the current is highly rectified even in 3 M KCl solution, with the rectification ratio up to ca. 49.7 (Fig. 3, B and C). Compared with other heterogeneous membranes, the critical concentration peak (the concentration where the highest rectification ratio appears) shifted to higher salt concentration at least by one order of magnitude (*19*, *22*, *23*, *37*). This result provides direct evidence that the Janus membrane could be used in the osmotic power conversion, as it still works in extremely high salt concentrations. To further understand the mechanism of this phenomenon, we take the numerical simulation to quantify the ion transport mechanism through the Poisson and Nernst-Plank (PNP) equations. For the self-assembly of ionomer membranes, no ICR phenomenon exists, indicating the 3D symmetry pore structure. However, the 3D porous networks are too sophisticated to build a model. Here, for simplicity, we take the 2D model for the Janus membrane 3D system (fig. S10). The simulated results demonstrate that the peak of the highest rectification ratio shifts from low to high concentration with increasing surface charge density (fig. S11).

We attribute this unique ICR in extremely high salt solution to small pores with narrow distribution and abundant surface charge of PAEK-HS, as each pendant bears six charges. The surface charge densities of HS20 and PES-Py are estimated to be −0.2 and 0.05 C/m^2, respectively. Connected pores of HS20 are considered as a cylindrical shape with ca. 18 nm in size and 400 nm in length, while the pores of PES-Py are set as a cylindrical tube with ca. 4 nm in radius and 40 nm in length. Figure 3D shows the ion concentration profile (C_p stands for the K^+ ion, and C_n refers to the Cl^- ion) along the channels. The insets of the concentration profile in Fig. 3D demonstrate, along the junction of HS20/PES-Py, that the ions are highly enriched under negative bias and depleted under positive bias in 1 M KCl solution. The asymmetric factors (surface charge polarity and density, pore size, and length) ensure that the ICR appears under high salt concentrations.

Then, the ionic transport through the Janus membrane was tested using an asymmetric electrolyte solution in an electrochemical testing setup (fig. S12). The high and low concentrations of KCl solutions were 1 M and 10 μM, respectively. With the high concentration of KCl solution on the PES-Py side, the absolute values of I_{short} (short-circuit current) and V_{open} (open-circuit voltage) were 0.51 μA and 0.31 V, respectively, while in the asymmetric electrolyte solution, the absolute values of I_{short} and V_{open} were 0.35 μA and 0.28 V, respectively (Fig. 3E). This means that when the high concentration of the solution is on the PAEK-HS side, the inner resistance of the Janus membrane increased by approximately 31.62%. Our numerical simulation results also proved that the preferential direction is that ions move from the PES-Py side to the PAEK-HS side. Under the

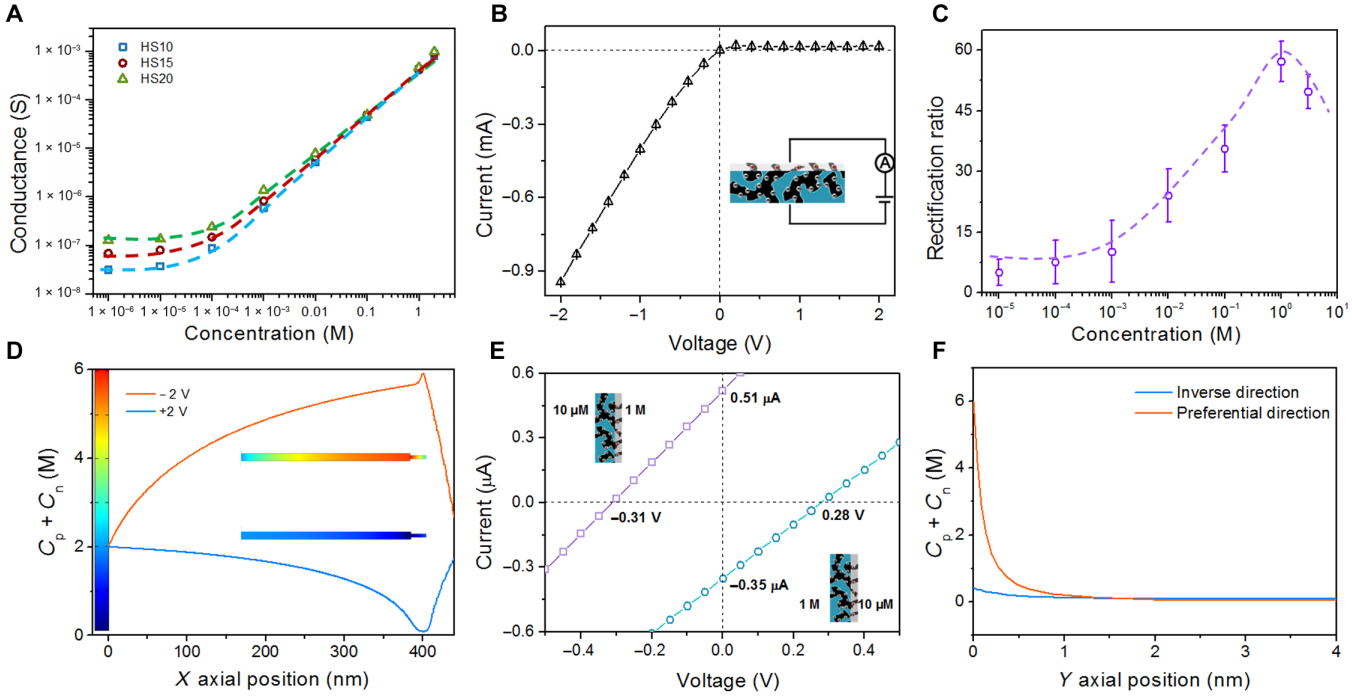

Fig. 3. The ionic transmembrane property of the Janus membrane. (**A**) Conductance versus salt concentration for various Janus membranes with HS10, HS15, and HS20 at pH 5. (**B**) Representative rectification *I-V* curve in 3 M KCl. The anode is on the PES-Py side, and the cathode is on the HS20 side. (**C**) Rectification ratio of the HS20 Janus membrane under a series of KCl solution concentration with pH 5. (**D**) Numerical simulation results of the ionic concentration distribution along the *X* axial position at −2 V and +2 V of the theoretical 1D model. The *X* = 0 nm position refers to the PAEK-HS side. The inset shows the calculated ion concentration profile. (**E**) *I-V* curves of the Janus membrane under two different configurations for the placement of electrolyte solutions. With the high concentration of KCl solution on the PES-Py side, the absolute value of I_{short} increases by approximately 40%. The high and low concentrations of KCl solutions are 1 M and 10 μM, respectively. (**F**) Numerical simulation results of the ionic concentration distribution along the *Y* axial position at the end of the low concentration solution. The preferential directions are the high concentration of the solution on the PES-Py side and the low concentration of the solution on the PAEK-HS side. The *Y* = 0 nm position refers to the surface of the channels along the radial direction.

seawater/river salinity gradient, the ionic concentration distributions and current were simulated in the steady state. The ionic concentration profiles along the "leave port" (the side with low ionic concentration) are shown in Fig. 3F. Obviously, many more ions move from the seawater to the river when the seawater is next to PES-Py. The calculated current in the direction from PES-Py to HS20 is 4.2 times of that in the reverse direction. These data suggested that the ICR still exists in this salinity gradient, ensuring the power conversion efficiency. The "preferential direction" for ion transport under the salinity gradient is with the PES-Py side fixing on the high salt solution; thus, the data presented are all recorded in this direction. In addition, we tested the current in different salinity gradients. The results demonstrated that both E_{open} and I_{short} of membranes increased with the increasing concentration gradients (fig. S13).

In addition, the Janus membrane still holds excellent ion selectivity in high salt solution. The selectivity of the membrane is tested by a visual experiment. Two oppositely charged fluorescent dyes (negatively charged sulfonated rhodamine and positively charged propidium iodide) marked the membrane at the preferential direction. As shown in fig. S14, the negatively charged dyes are permeable across the membrane, while the positively charged dyes are excluded from the membrane. Thus, the Janus membrane works as an anion selector. Moreover, this anion selectivity is quantitatively characterized by the transference number (t_n; it equals 1 for ideal anion selective case) (*14*), and the data at different salinity gradients are listed in table S2. Selectivity still works in hypersaline solution beyond the concentration limitation. Even in asymmetric salt solution with 1 M/10^{-5} M, t_n of up to 0.882 is still maintained. In the asymmetric seawater and river water salinity gradient, the transference number is 0.923. This highly effective selectivity within preferential ionic transport direction would benefit the energy conversion process, and thus, high efficiency is expected.

Osmotic power conversion through the Janus membrane

The harvested electric power is estimated by transferring it to an external circuit with an electric load resistor (R_L; inset in Fig. 4A). We systematically explored the current density and output power of the Janus membrane as functions of load resistance and membrane resistance. The power density of the resistor in the circuit is calculated using the equation $P_L = I^2_{osmosis}R_L$. With the increasing load resistance, the current density is reduced (Fig. 4A) and the output power reaches a maximum at the resistance, which is equal to that of the membrane (Fig. 4B). Notably, the resistance of the Janus membrane, as shown in Fig. 4B (the point where $R_M = R_L$), was much reduced with the increasing pendant proportions. The resistance of PES-Py/HS10 increases by 76% compared to that of PES-Py/HS20, while the output power density of PES-Py/HS10 decreases by 42%. With lowest resistance, the maximum output power density of the generator based on the PES-Py/HS20 membrane reached up to 2.6 W/m^2. These data were in accordance with the porosity variation and indicate that the output power density could be modulated by tuning the porosity of the porous membrane. This also proves that our method is an effective route to prepare the porous membrane.

We then proceeded to test how the concentration gradient affects energy conversion carried out by the Janus membrane, and we obtained the data from the Janus PES-Py/HS20 membrane, as shown in Fig. 4 (D to F). The low-salinity solution was placed in the HS20

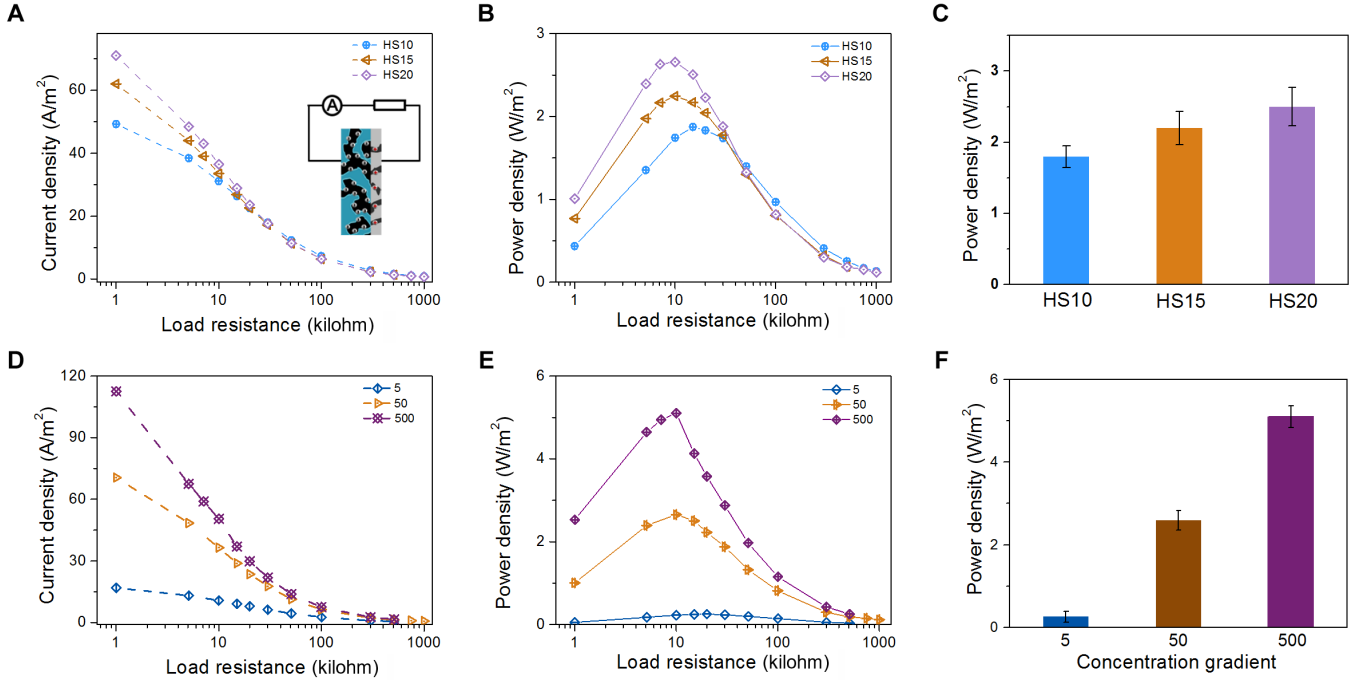

Fig. 4. Ultrahigh output power density of the Janus 3D porous membrane–based osmotic power generator. The collected power is transferred to the external circuit to supply an electronic load (inset). (**A** and **B**) Current density and output power of PES-Py/HS10, PES-Py/HS15, and PES-Py/HS20 as functions of load resistance. The PES-Py side was placed to artificial seawater (0.5 M NaCl), while the PAEK-HS side was placed to artificial river water (0.01 M NaCl). With increasing load resistance, the current density is reduced and the output power reaches a maximum at a moderate resistance. (**C**) The maximum output power density goes up with the increasing pendant proportion. The maximum PES-Py/HS20 is about 2.6 W/m^2. (**D** and **E**) Current density and output power of HS20 as functions of load resistance under three salinity gradients. The low-salinity solution was placed in the PAEK side and fixed at 0.01 M. High-salinity solution is tunable from 0.05 to 5 M NaCl. (**F**) With increased salinity gradients, the output power density goes up and reaches a maximum at a 500-fold salinity gradient. The maximum value is 5.10 W/m^2.

side with 0.01 M NaCl, and the high-salinity solution was varied from 0.05 to 5 M NaCl. With increasing salinity gradients, the output power density went up and reached a maximum at a 500-fold salinity gradient. As expected, the Janus membrane works in high salt solution, and the maximum value of the output power density reached up to 5.10 W/m^2. The performance of the Janus membrane generator would enable it to collect energy along the side where the salt lake meets the river. In addition, the performance of the membrane in seawater environment (pH is ca. 8) is tested, and the power density is still up to 1.7 W/m^2 (fig. S15).

Furthermore, the efficiency is much enhanced, attributed to the effective rectified current and selectivity in hypersaline solution, which is up to 35.7% by mixing the seawater and river water (table S2). Compared with the other heterogeneous membranes (*19*, *20*, *38*), where efficiencies decreased sharply with an increasing concentration gradient, our Janus membrane harvested up to 29.2% energy in an asymmetric salt solution of 1 M/10^{-5} M. These results are in accordance with the rectified current and high selectivity in hypersaline solution.

Robustness and high endurance of the Janus membrane

Sufficient mechanical properties of the Janus membranes are one of the key requirements for their large-scale practical applications. All the copolymers in the Janus membranes have high-temperature thermostability, as onset weight loss temperatures are higher than 200°C, as shown in the thermogravimetric analysis (TGA) curves (Fig. 5A). Furthermore, the swelling ratio is less than 10% even at 80°C (Fig. 5B). Along with the increasing pendant proportion in PAEK-HS, the tensile strength decreased, while the membrane displayed larger elongation at break (Fig. 5, C and D). This is largely due to the introduction of large side chains, which restrain orderly arrangement of the polymer main chain. In addition to the molecular structure, the mechanical properties are also related to the operating environment. Water leads to a marked improvement of membrane flexibility and a decrease of material rigidity. Taking the PES-Py/HS20 membrane as an example, we observed that the tensile strength decreased by 18% from the dry state to the wet state, while the elongation at break increased by 32%. For a visual demonstration, a 0.02 mm–by–5 mm sample could hang about 300 g of weight (Fig. 5E). These results indicate that Janus membranes as energy-harvesting devices are sufficiently tough and ductile enough for large-scale practical applications.

High endurance of high-performance generator

Here, we construct a tandem Janus 3D porous membrane–based generator to demonstrate the performance of the membrane. The prepared generator could directly power a calculator in a long-term run (Fig. 5F). The output voltages showed a perfect linear relationship

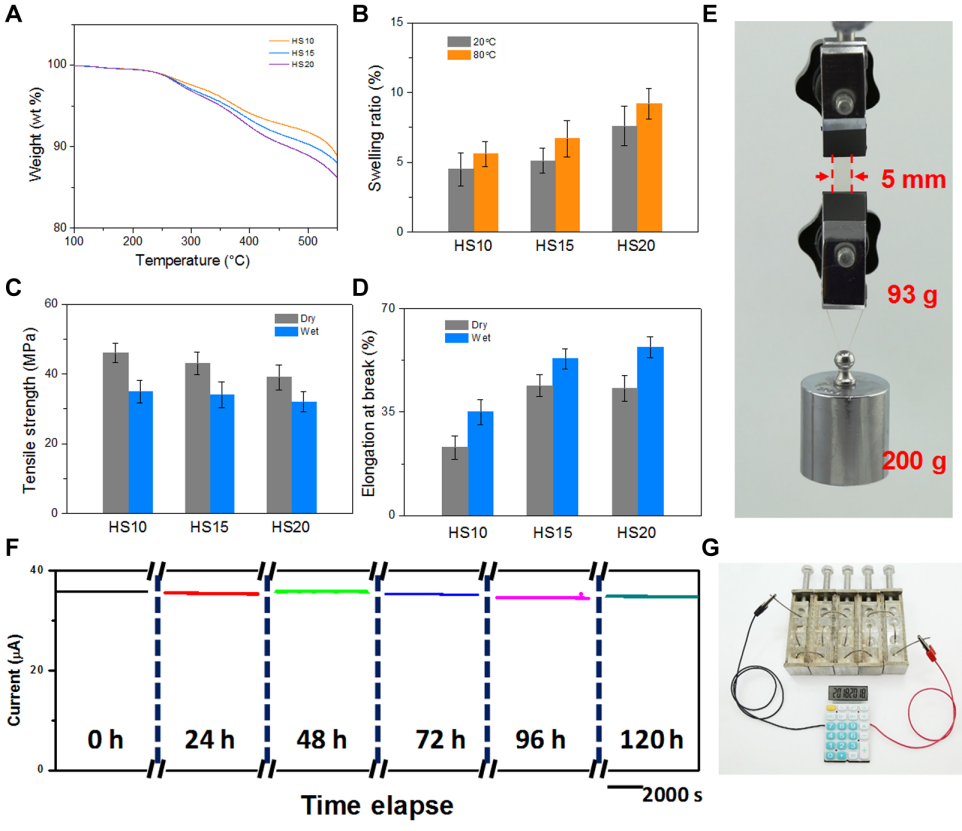

Fig. 5. The robustness and high endurance of a high-performance generator based on the Janus membrane. (**A**) TGA curves of Janus membranes. The onset weight loss temperatures were higher than 200°C. (**B**) Swelling ratio of membranes at 20° and 80°C. The swelling is more pronounced by increasing the proportion of hydrophilic pendant. (**C**) Tensile strength of dry and wet membranes. (**D**) Elongation at break of dry and wet membranes. With increasing pendent proportion, the tensile strength is reduced, while the membrane displays a higher elongation at break. (**E**) A 0.02 mm–by–5 mm membrane can hang about 300 g of weight. (**F**) Time series of the current of the Janus membrane–based energy devices by mixing artificial river water and artificial seawater. (**G**) Tandem Janus membrane–based power generator can directly power a calculator.

of 150 mV per single unit cell under a river water (0.01 M NaCl) and seawater (0.5 M NaCl) salinity gradient (fig. S16). Within 120 hours under the seawater/river water salinity gradient, the current did not decline (Fig. 5G), which demonstrated robustness and high endurance of the Janus 3D membrane–based generator. Compared to the post-functioned surface charge density in as-prepared nanochannels, the surface charges in ionomers are strictly confined along the pores. In addition to the rigid backbone, the Janus membrane–based generator, as expected, has excellent robustness and long-term persistent properties. This also ensures that the application of the membrane-based generator is viable.

DISCUSSION

Here, a high-performance Janus membrane–based generator is successfully built, and a new point of view is proposed in our work. To avoid the ion polarization phenomenon in a single-layer membrane, we integrated nonlinear current into the energy conversion system. The Janus membrane with rectified current carries the ions as an "ion-express highway" from the seawater to the river. To maintain high-conversion efficiency, ICR in extremely high salt concentration is desired. With a chemical molecule design, the porosity and surface charge density are both tuned, which benefits ionic conductance (*24*) and rectified current phenomenon. To the best of our knowledge, the working concentration zone (the maximum rectification ratio appears at 1 M KCl) breaks the concentration limitation and shifts to higher concentration at least by one order of magnitude. Effective ion selectivity and rectified current (nonlinear ionic transport) in hypersaline solution ensure the high performance of osmotic energy conversion. In addition, massive ionic flow is achieved by tuning surface charge density and porosity, improving power density. The osmotic conversion power densities are up to 2.66 W/m^2 (by mixing seawater and river water with 35.7% efficiency) and 5.10 W/m^2 (at a 500-fold salinity gradient). Furthermore, the practical application issues have also been considered. With a chemical molecule design, a large-scale membrane with excellent robustness is readily obtained. Our work predicts that the diode current–type membrane holds great potential in collecting blue energy, and understanding of ionic transport in confined nanoenvironment reveals a new chapter in porous material design.

MATERIALS AND METHODS

Synthesis of PAEK-HS

The charge density plays a very important role in our system. To increase the charge density, we designed a monomer containing hexaphenylbenzene that can be highly sulfonated. The PAEK-HS was synthesized by an aromatic nucleophilic substitution polymerization reaction. Carbonyl, a strong electron-withdrawing group, was introduced to activate the aromatic dihalides. In addition, we built an aliphatic bridge between the hydrophobic main chain and hydrophilic sulfonated hexaphenylbenzene to increase the flexibility of side chains, which is more advantageous for the phase separation. The PAEK-HS with different proportions of hexaphenylbenzene could be synthesized by controlling the rate of the monomer accurately.

Fabrication of Janus 3D porous membrane

The sulfonated polymers were dissolved in dimethylacetamide (DMAc). The membrane was prepared by pouring sulfonated copolymer solutions onto a leveled clean glass plates after filtration. The removal of DMAc was accomplished by drying at 60°C for 15 hours and under vacuum at 120°C for 15 hours. After cooling to room temperature, the PES-Py solution in $CHCl_3$ was spin-coated on the as-prepared membrane, dried at 45°C in a vacuum oven for 12 hours, and peeled off. The copolymer self-assembled into the 3D porous membrane via micro-/nanophase separation. The membrane thickness can be controlled by adjusting the concentration of the polymer.

Numerical simulation

The ionic concentration and current distribution in steady state were calculated by the 2D PNP equation using the commercial finite-element package COMSOL Multiphysics (version 4.4). Considering the 3D symmetric structure in PAEK-HS and PES-Py, the Janus membrane was simplified as the 2D model (fig. S10).

SUPPLEMENTARY MATERIALS

Supplementary material for this article is available at http://advances.sciencemag.org/cgi/content/full/4/10/eaau1665/DC1

Section S1. The optical photograph of the Janus nanoporous membrane
Section S2. Materials
Section S3. Measurements
Section S4. Synthesis of PAEK-HS
Section S5. Synthesis of PES-Py
Section S6. Characterization of PAEK-HS
Section S7. Characterization of PES-Py
Section S8. Inherent viscosity of the copolymers
Section S9. FT-IR spectra of PAEK-HS
Section S10. Porosity and pore size distribution
Section S11. Zeta potential of PAEK-HS
Section S12. Ion exchange capacity
Section S13. Model building
Section S14. Experimental setup
Section S15. The effect of the concentration gradients on short-circuit current and open-circuit voltage
Section S16. Ion selectivity of the membrane
Section S17. Energy conversion efficiency
Section S18. Fabrication of Janus heterogeneous membrane
Section S19. The performance of the membrane under neutral
Section S20. Tandem membrane-based power electronic devices
Section S21. Electrode calibration
Fig. S1. Digital photo of the large-scale Janus nanoporous membrane with an approximate thickness of 11 μm.
Fig. S2. ^1H NMR spectra (500 MHz, $CDCl_3$, room temperature) of monomer.
Fig. S3. ^1H NMR spectra (500 MHz, DMSO-d_6, room temperature) of PAEK-HS15.
Fig. S4. ^1H NMR spectra (500 MHz, DMSO-d_6, room temperature) of monomer.
Fig. S5. ^1H NMR spectra (500 MHz, DMSO-d_6, room temperature) of PES-Py.
Fig. S6. FT-IR spectra of PAEK-HP and PAEK-HS with different proportions of hydrophilic high concentration of sulfonated side chain (from top to bottom: 10, 15, and 20%, respectively).
Fig. S7. The histogram of pore size distribution with Gaussian fit.
Fig. S8. The zeta potential of membranes PAEK-HS10, PAEK-HS15, and PAEK-HS20.
Fig. S9. The ion exchange capacity values of the sulfonated membranes.
Fig. S10. Numerical simulation model based on PNP theory.
Fig. S11. Numerical simulation results of the effect of the surface charge density on the ICR ratio.
Fig. S12. Schematic of the electrochemical testing setup.
Fig. S13. V_{open} and I_{short} of HS10, HS15, and HS20 under various concentration gradients (KCl).
Fig. S14. Visual experiment for the selectivity.
Fig. S15. The output power and current density of PES-Py/HS20 under a series of external load resistance at pH 7.4.
Fig. S16. *I-V* curves of the 10 units' device under river water (0.01 M NaCl) on the HS side and seawater (0.5 M NaCl) on the Py side.
Fig. S17. The equivalent circuit diagram of the testing system.
Scheme S1. Synthesis of PAEK-HS.
Scheme S2. Synthesis of PES-Py.
Table S1. Inherent viscosity of the copolymers.
Table S2. The conversion efficiency of the Janus membrane at different salinity gradients.
Table S3. V, E_{Redox}, and E_{Diff} of HS10, HS15, and HS20.
References (*39*, *40*)

REFERENCES AND NOTES

1. M. Elimelech, W. A. Phillip, The future of seawater desalination: Energy, technology, and the environment. *Science* **333**, 712–717 (2011).
2. B. E. Logan, M. Elimelech, Membrane-based processes for sustainable power generation using water. *Nature* **488**, 313–319 (2012).
3. G. Z. Ramon, B. J. Feinberg, E. M. V. Hoek, Membrane-based production of salinity-gradient power. *Energy Environ. Sci.* **4**, 4423–4434 (2011).
4. J. R. Werber, C. O. Osuji, M. Elimelech, Materials for next-generation desalination and water purification membranes. *Nat. Rev. Mater.* **1**, 16018 (2016).
5. A. Cipollina, M. Giorgio, *Sustainable Energy from Salinity Gradients* (Woodhead Publishing, 2016).
6. R. E. Pattle, Production of electric power by mixing fresh and salt water in the hydroelectric pile. *Nature* **174**, 660 (1954).
7. S. Loeb, R. S. Norman, Osmotic power plants. *Science* **189**, 654–655 (1975).
8. A. Siria, M.-L. Bocquet, L. Bocquet, New avenues for the large-scale harvesting of blue energy. *Nat. Rev. Chem.* **1**, 0091 (2017).
9. J. W. Post, J. Veerman, H. V. M. Hamelers, G. J. W. Euverink, S. J. Metz, K. Nymeijer, C. J. N. Buisman, Salinity-gradient power: Evaluation of pressure-retarded osmosis and reverse electrodialysis. *J. Membr. Sci.* **288**, 218–230 (2007).
10. M. Turek, B. Bandura, Renewable energy by reverse electrodialysis. *Desalination* **205**, 67–74 (2007).
11. A. Achilli, A. E. Childress, Pressure retarded osmosis: From the vision of Sidney Loeb to the first prototype installation—Review. *Desalination* **261**, 205–211 (2010).
12. K. L. Lee, R. W. Baker, H. K. Lonsdale, Membranes for power generation by pressure-retarded osmosis. *J. Membr. Sci.* **8**, 141–171 (1981).
13. J. Ji, Q. Kang, Y. Zhou, Y. Feng, X. Chen, J. Yuan, W. Guo, Y. Wei, L. Jiang, Osmotic power generation with positively and negatively charged 2D nanofluidic membrane pairs. *Adv. Funct. Mater.* **27**, 1603623 (2017).
14. D.-K. Kim, C. Duan, Y.-F. Chen, A. Majumdar, Power generation from concentration gradient by reverse electrodialysis in ion-selective nanochannels. *Microfluid. Nanofluid.* **9**, 1215–1224 (2010).
15. T. B. H. Schroeder, A. Guha, A. Lamoureux, G. VanRenterghem, D. Sept, M. Shtein, J. Yang, M. Mayer, An electric-eel-inspired soft power source from stacked hydrogels. *Nature* **552**, 214–218 (2017).
16. P. Długołęcki, K. Nymeijer, S. Metz, M. Wessling, Current status of ion exchange membranes for power generation from salinity gradients. *J. Membr. Sci.* **319**, 214–222 (2008).
17. J. G. Hong, B. Zhang, S. Glabman, N. Uzal, X. Dou, H. Zhang, X. Wei, Y. Chen, Potential ion exchange membranes and system performance in reverse electrodialysis for power generation: A review. *J. Membr. Sci.* **486**, 71–88 (2015).
18. C. B. Picallo, S. Gravelle, L. Joly, E. Charlaix, L. Bocquet, Nanofluidic osmotic diodes: Theory and molecular dynamics simulations. *Phys. Rev. Lett.* **111**, 244501 (2013).
19. Z. Zhang, X. Y. Kong, K. Xiao, Q. Liu, G. Xie, P. Li, J. Ma, Y. Tian, L. Wen, L. Jiang, Engineered asymmetric heterogeneous membrane: A concentration-gradient-driven energy harvesting device. *J. Am. Chem. Soc.* **137**, 14765–14772 (2015).
20. Z. Zhang, X. Sui, P. Li, G. Xie, X. Y. Kong, K. Xiao, L. Gao, L. Wen, L. Jiang, Ultrathin and ion-selective Janus membranes for high-performance osmotic energy conversion. *J. Am. Chem. Soc.* **139**, 8905–8914 (2017).
21. R. Karnik, C. Duan, K. Castelino, H. Daiguji, A. Majumdar, Rectification of ionic current in a nanofluidic diode. *Nano Lett.* **7**, 547–551 (2007).
22. R. Yan, W. Liang, R. Fan, P. Yang, Nanofluidic diodes based on nanotube heterojunctions. *Nano Lett.* **9**, 3820–3825 (2009).
23. X. Zhu, Y. Zhou, J. Hao, B. Bao, X. Bian, X. Jiang, J. Pang, H. Zhang, Z. Jiang, L. Jiang, A charge-density-tunable three/two-dimensional polymer/graphene oxide heterogeneous nanoporous membrane for ion transport. *ACS Nano* **11**, 10816–10824 (2017).
24. A. Siria, P. Poncharal, A. L. Biance, R. Fulcrand, X. Blase, S. T. Purcell, L. Bocquet, Giant osmotic energy conversion measured in a single transmembrane boron nitride nanotube. *Nature* **494**, 455–458 (2013).
25. C. Lee, L. Joly, A. Siria, A. L. Biance, R. Fulcrand, L. Bocquet, Large apparent electric size of solid-state nanopores due to spatially extended surface conduction. *Nano Lett.* **12**, 4037–4044 (2012).
26. L. Bocquet, E. Charlaix, Nanofluidics, from bulk to interfaces. *Chem. Soc. Rev.* **39**, 1073–1095 (2010).
27. K. Schmidt-Rohr, Q. Chen, Parallel cylindrical water nanochannels in Nafion fuel-cell membranes. *Nat. Mater.* **7**, 75–83 (2008).
28. A. Kusoglu, A. Z. Weber, New insights into perfluorinated sulfonic-acid ionomers. *Chem. Rev.* **117**, 987–1104 (2017).
29. X. Hou, Y. S. Zhang, G. Trujillo-de Santiago, M. M. Alvarez, J. Ribas, S. J. Jonas, P. S. Weiss, A. M. Andrews, J. Aizenberg, A. Khademhosseini, Interplay between materials and microfluidics. *Nat. Rev. Mater.* **2**, 17016 (2017).
30. X. Hou, H. C. Zhang, L. Jiang, Building bio-inspired artificial functional nanochannels: From symmetric to asymmetric modification. *Angew. Chem. Int. Ed.* **51**, 5296–5307 (2012).
31. L. Wen, X. Hou, Y. Tian, J. Zhai, L. Jiang, Bio-inspired photoelectric conversion based on smart-gating nanochannels. *Adv. Funct. Mater.* **20**, 2636–2642 (2010).
32. M. R. Powell, I. Vlassiouk, C. Martens, Z. S. Siwy, Nonequilibrium 1/f noise in rectifying nanopores. *Phys. Rev. Lett.* **103**, 248104 (2009).
33. D. Constantin, Z. S. Siwy, Poisson-Nernst-Planck model of ion current rectification through a nanofluidic diode. *Phys. Rev. E* **76**, 041202 (2007).
34. P. Y. Apel, Y. E. Korchev, Z. Siwy, R. Spohr, M. Yoshida, Diode-like single-ion track membrane prepared by electro-stopping. *Nucl. Instrum. Methods Phys. Res. Sect. B* **184**, 337–346 (2001).
35. M. Ali, S. Mafe, P. Ramirez, R. Neumann, W. Ensinger, Logic gates using nanofluidic diodes based on conical nanopores functionalized with polyprotic acid chains. *Langmuir* **25**, 11993–11997 (2009).
36. X. Li, T. Zhai, P. Gao, H. Cheng, R. Hou, X. Lou, F. Xia, Role of outer surface probes for regulating ion gating of nanochannels. *Nat. Commun.* **9**, 40 (2018).
37. Z. Zhang, X.-Y. Kong, K. Xiao, G. Xie, Q. Liu, Y. Tian, H. Zhang, J. Ma, L. Wen, L. Jiang, A bioinspired multifunctional heterogeneous membrane with ultrahigh ionic rectification and highly efficient selective ionic gating. *Adv. Mater.* **28**, 144–150 (2016).
38. J. Gao, W. Guo, D. Feng, H. Wang, D. Zhao, L. Jiang, High-performance ionic diode membrane for salinity gradient power generation. *J. Am. Chem. Soc.* **136**, 12265–12272 (2014).
39. H. S. White, A. Bund, Ion current rectification at nanopores in glass membranes. *Langmuir* **24**, 2212–2218 (2008).
40. J. Cervera, B. Schiedt, R. Neumann, S. Mafé, P. J. Ramírez, Ionic conduction, rectification, and selectivity in single conical nanopores. *J. Chem. Phys.* **124**, 104706 (2006).

Acknowledgments: The preparation of ionomers, chemical structure characterization, and stress-strain tests were performed in Jilin University. The fabrication of porous membrane and ionic transmembrane tests were performed in the Key Laboratory of Bio-inspired Materials and Interfacial Science, Technical Institute of Physics and Chemistry. We appreciated the discussion with J. Zhou and Ph.D. candidate Y. Wang in Beihang University. **Funding:** This work was supported by the Key Research Program of the Chinese Academy of Sciences (KJZD-EW-M03), National Science Foundation of China (21875270, 21504097, and 21774048), and Frontier Science Key Projects of CAS (QYZDY-SSW-SLH014). **Author contributions:** Y.Z. and L.J. conceived the idea. Y.Z., L.J., and X.Z. designed the research. X.Z. and J.P. performed the experiments. X.Z., J.H., Y.Z., and L.J. analyzed and interpreted the results. Y.Z., L.J., and X.Z. drafted the manuscript. B.B. and H.Z. carried out material preparation. Y.Z., L.J., and Z.J. supervised the project. All authors contributed to the writing of the manuscript. **Competing interests:** The authors declare that they have no competing interests. **Data and materials availability:** All data needed to evaluate the conclusions in the paper are present in the paper and/or the Supplementary Materials. Additional data related to this paper may be requested from the authors.

Submitted 14 May 2018
Accepted 19 September 2018
Published 26 October 2018
10.1126/sciadv.aau1665

Citation: X. Zhu, J. Hao, B. Bao, Y. Zhou, H. Zhang, J. Pang, Z. Jiang, L. Jiang, Unique ion rectification in hypersaline environment: A high-performance and sustainable power generator system. *Sci. Adv.* **4**, eaau1665 (2018).

Unique ion rectification in hypersaline environment: A high-performance and sustainable power generator system

Xuanbo Zhu, Junran Hao, Bin Bao, Yahong Zhou, Haibo Zhang, Jinhui Pang, Zhenhua Jiang and Lei Jiang

Sci Adv **4** (10), eaau1665.
DOI: 10.1126/sciadv.aau1665